# Macroscopic modeling of variable speed limits on freeways

Dominguez Frejo, Jose Ramon; Papamichail, Ioannis; Papageorgiou, Markos; De Schutter, Bart

**DOI**
10.1016/j.trc.2019.01.001

**Publication date**
2019

**Document Version**
Final published version

**Published in**
Transportation Research Part C: Emerging Technologies

**Citation (APA)**
Dominguez Frejo, J. R., Papamichail, I., Papageorgiou, M., & De Schutter, B. (2019). Macroscopic modeling of variable speed limits on freeways. *Transportation Research Part C: Emerging Technologies*, *100*, 15-33. https://doi.org/10.1016/j.trc.2019.01.001

**Important note**
To cite this publication, please use the final published version (if applicable).
Please check the document version above.

Transportation Research Part C 100 (2019) 15–33

Contents lists available at ScienceDirect

Transportation Research Part C

journal homepage: www.elsevier.com/locate/trc

# Macroscopic modeling of variable speed limits on freeways

José Ramón D. Frejo[a], Ioannis Papamichail[b], Markos Papageorgiou[b], Bart De Schutter[a]

[a] Delft Center for Systems and Control, Delft University of Technology, the Netherlands
[b] Dynamic Systems and Simulation Laboratory, Technical University of Crete, Chania, Greece

ARTICLE INFO

*Keywords:*
Variable speed limit
Freeway traffic control
Modeling
Macroscopic traffic flow models
METANET

ABSTRACT

The goals of this paper are to analyze the effects of Variable Speed Limits (VSLs) on freeway traffic flow, to propose a new macroscopic model for VSL, and to compare, calibrate and validate the most well known macroscopic models for VSL using real data from a stretch of the A12 freeway in The Netherlands.

Firstly, a new macroscopic model for VSLs is presented, combining characteristics of previously proposed models, in order to have the capability of modeling different capacities, critical densities, and levels of compliance for segments affected by speed limits. Subsequently, the effects of VSLs on the fundamental diagram of traffic flow are studied concluding that, at least for the considered stretch of the A12 freeway, the capacity of the freeway segment is decreased (and the critical density is increased) when the speed limit is reduced from 120 to 90 km/h. Furthermore, analyzing a wider range of VSLs, it is shown that the VSL-induced fundamental diagram is not triangular and that the speed limit compliance can be very low if enforcement measures are not applied. Finally, the proposed model is compared analytically, numerically, and graphically with the two most well-known macroscopic models for VSLs. The analysis and the simulation results show that the proposed model delivers more accurate predictions in cases where the compliance is low and/or the capacity is reduced by the use of VSLs.

## 1. Introduction

Nowadays, many social and economic problems such as waste of time and fuel, greater accident risks, and an increase in pollution are caused by traffic jams on freeways. Due to economic or viability reasons, the construction of new freeways is not always the best solution. One promising alternative is the use of dynamic control signals such as ramp metering, reversible lanes, and route guidance. Besides these traffic control measures, in the past years, Variable Speed Limits (VSLs) have emerged as a potential traffic management measure for increasing freeway efficiency. The first implementation of VSLs dates back to 1970 in Germany (Zackor, 1972). During the subsequent decades, VSLs have been also applied in The Netherlands, United States, and other countries (Sumner and Andrew, 1990; van den Hoogen and Smulders, 1994).

Earlier studies assumed that, if a VSL is applied, the capacity of a freeway segment is increased due to speed harmonization within each lane and across different lanes (Zackor, 1972; Cremer, 1979). Thus, the main objective, beyond improving traffic safety, was to increase freeway efficiency by applying VSLs to congested bottlenecks. However, later works did not identify any capacity increase due to VSLs (Smulders, 1990; van den Hoogen and Smulders, 1994; Papageorgiou et al., 2008; Soriguera et al., 2017); even a slight

*E-mail addresses:* jdominguez3@us.es (J.R. D. Frejo), ipapa@dssl.tuc.gr (I. Papamichail), markos@dssl.tuc.gr (M. Papageorgiou), B.DeSchutter@tudelft.nl (B. De Schutter).

https://doi.org/10.1016/j.trc.2019.01.001
Received 14 March 2018; Received in revised form 4 December 2018; Accepted 3 January 2019
Available online 18 January 2019
0968-090X/ 

capacity reduction is observed concluding that a substantial improvement of the traffic efficiency cannot be reached by applying VSLs to increase capacity at congested bottlenecks. Furthermore, in a recent work (Soriguera et al., 2016), a significant capacity reduction (around 15%) is observed when low sub-critical speed limits are applied.

Consequently, nowadays, three kinds of VSL control algorithms are considered in the literature (a review about the use of VSLs for freeway traffic control can be found in Lu and Shladover (2014)):

- **Safety-oriented VSLs:** This kind of VSL control algorithms are applied in order to increase traffic safety by reducing the speed limit when a vehicle is approaching a congested segment or an incident. The safety benefits of these control algorithms have been reported in field studies (with a 30% reduction in the number of crashes (Robinson, 2000)). However, these applications have not yet achieved a significant improvement of flow or capacity.
- **VSLs for traffic efficiency improvement:**
  - **Homogenization techniques:** Based on the idea that lower speed limits promote the reduction of fluctuations in traffic behavior and, therefore, the increase of bottleneck capacity, researches (Smulders, 1990; van den Hoogen and Smulders, 1994) proposed VSL control algorithms focused on the concept of homogenization, using VSLs around the critical speed.
  - **VSLs for traffic efficiency improvement by mainline metering:** The goal of these VSL control algorithms is to avoid, resolve, or reduce traffic jams on freeways by limiting the arriving flow and, thereby, avoiding or mitigating the capacity drop (Hegyi et al., 2005; Hegyi et al., 2008; Carlson et al., 2010, 2011; Frejo and Camacho, 2012; Frejo et al., 2014; Frejo and De Schutter, 2018). These techniques have been mainly tested by simulation and, therefore, their potential improvement in the traffic conditions relies on the model used. Moreover, the use of model-based optimal control algorithms (like Model Predictive Control (MPC) (Camacho and Bordons, 2010)) can considerably improve the Total Time Spent (TTS), emissions, fuel consumption, and other traffic performance indices, but their success highly depends on model accuracy (Hegyi et al., 2005; Frejo and Camacho, 2012).
- **Pollution-oriented algorithms:** Pollution-oriented VSL control algorithms, usually based on the structure of a controller designed for traffic efficiency improvement, provide a balanced trade-off between travel times, fuel consumption, and emissions. However, as indicated in Zegeye et al. (2012), the reduction of the emissions that can achieved without decreasing traffic efficiency is usually relatively low (2.5% for the case study used in Zegeye et al. (2012)).

One of the few empirically tested VSL control strategies for traffic efficiency improvement was the SPECIALIST algorithm which was applied at the A12 freeway in The Netherlands during 2009–10 (Hegyi and Hoogendoorn, 2010). However, this work focuses on the performance of the SPECIALIST algorithm without analyzing in depth the modeling of the effects of Variable Speed Limits (VSLs). On the other hand, the main goal of this paper is to use the field data available from the SPECIALIST field test in order to study in detail the effects of VSLs on freeways. Moreover, a new model for VSLs is proposed in this paper in order to have a better fit of the traffic data.

The main contributions of this paper with respect to the state-of-the-art are:

- The proposal of a new macroscopic model for VSLs combining characteristics of the previously proposed models.
- To carry out the first calibration and validation (using real data) of the most well-known macroscopic traffic flow models for VSLs.
- To perform an in depth comparison of those most well known macroscopic traffic flow models, including an analysis of the effects of VSLs on the capacity and critical density of a segment.

Note that although a basic version of the new macroscopic model was already introduced in the conference paper (Frejo et al., 2018), in this paper we extend it providing a detailed account and motivation of the model. In addition, we also calibrate and validate the new model.

The paper is structured as follows. Section 2 introduces the general formulation of the macroscopic model METANET without considering VSLs. Section 3 shows the two main ways of modeling VSLs within METANET and proposes a new one. Section 4 summarizes the main characteristics of the network and the data set used. Sections 5 and 6 analyze, respectively, the capacity reduction and the free flow response induced by the VSLs based on Fundamental Diagram (FD) measurements. Section 7 presents the calibration of the model parameters for the morning period of one congested day. This calibration is validated for the same time period of other days in Section 8 and for short periods of time for which the SPECIALIST algorithm is applied in Section 9. Finally, conclusions are drawn in Section 10.

## 2. METANET model without VSL

In model-based freeway traffic control using VSLs, an accurate, but significantly faster than real-time, prediction model is necessary. Two main approaches are used for the traffic flow modeling:

- Microscopic models, which describe the longitudinal and lateral movement of individual vehicles.
- Macroscopic models, which mostly model traffic as a particular fluid with aggregate variables such as density, mean speed and flow.

One of the main advantages of microscopic models is their ability to study individual vehicle motion visually, perceiving the real

process using simulation software. However, microscopic models are difficult to use for model based control due to the computational effort needed; thus, these models are usually only used for simulation and off-line tuning of controllers. On the other hand, macroscopic models are more suitable for real-time applications because they are relatively fast and have an analytical form. This paper, therefore, focuses on the modeling of VSLs within the framework of macroscopic traffic models.

Within macroscopic traffic flow models, first-order models like the Cell Transmission Model (CTM) (Daganzo, 1994) include a static speed-density relationship. On the other hand, second-order models like METANET (Papageorgiou et al., 2010) address the speed as another state variable with an according state equation, which is capable of capturing additional dynamics and, more important, is able to model capacity drop (Yuan et al., 2015).

We have focused this work on the modeling of VSL by modifying the second-order model METANET. In any case, the analyzed models for the FD induced by the VSLs could be included within other 1st and 2nd order macroscopic model. For instance, the CTM model could be modified in order to include the effect of VSL by adjusting the supply and demand functions.

Apart from VSLs, METANET can handle other control actions such as ramp metering (Papageorgiou et al., 1997), route guidance (Wang et al., 2006), and reversible lanes (Frejo et al., 2016). This allows the design and testing of integrated controllers (or independent controllers working in parallel) for many traffic control measures operating on the same network.

METANET represents the traffic network as a graph where the links (indexed by $m$) correspond to freeway stretches, which are divided into $N_m$ segments of length $L_m$ with $\lambda_m$ lanes. The traffic density $\rho_{m,i}(k)$ and the mean speed $v_{m,i}(k)$ dynamically characterize the state of each segment where $k$ is the time step corresponding to the time instant $t = kT$ and $T$ is the simulation time step. From now on, all segments will be considered to have different lengths and, therefore $N_m = 1\ \forall\ m$, making it unnecessary to differentiate between links and segments; thus, hereafter only the index $i$ will be used.

Two main equations describe the system dynamics of METANET model. The first one expresses the conservation of vehicles:

$$\rho_i(k+1) = \rho_i(k) + \frac{T}{\lambda_i L_i}(q_{i-1}(k) - q_i(k) + q_{\mathrm{r},i}(k) - \beta_i(k) q_{i-1}(k)) \tag{1}$$

where $q_{\mathrm{r},i}(k)$ is the traffic flow that enters the freeway link $i$ from the connected on-ramp (if any) and $\beta_i(k)$ is the split ratio of the off-ramp (i.e. the percentage of vehicles exiting the freeway through the off-ramp in link $i$, if any). We set $\beta_i(k) = 0$ and $q_{r,i}(k) = 0$ for links without an off-ramp or an on-ramp, respectively. The leaving traffic flow at each link $q_i(k)$ can be computed for each time step using $q_i(k) = \lambda_i \rho_i(k) v_i(k)$.

The second equation expresses the mean speed as a sum of the previous mean speed, a relaxation term, a convection term, and an anticipation term:

$$v_i(k+1) = \max\Bigg(v_{\min},\ v_i(k) + \frac{T}{\tau_i}(V_i(k) - v_i(k)) + \\ + \frac{T}{L_i} v_i(k)(v_{i-1}(k) - v_i(k)) - \frac{\mu_i T}{\tau_i L_i}\frac{\rho_{i+1}(k) - \rho_i(k)}{\rho_i(k) + K}\Bigg) \tag{2}$$

where $\tau_i$, and $\mu_i$ are model parameters that have to be estimated for each link, $v_{\min}$ and $K$ are model parameters that are constant for all links, and $V_i(k)$ is the desired speed for the drivers that, in absence of VSL, is modeled by the following equation for a freeway segment $i$:

$$V_i(k) = v_{\mathrm{f},i} e^{-\frac{1}{a_i}\left(\frac{\rho_i(k)}{\rho_{\mathrm{c},i}}\right)^{a_i}} \tag{3}$$

where $a_i$ is a model parameter, $v_{\mathrm{f},i}$ is the free flow speed that the vehicles reach at zero density, and $\rho_{\mathrm{c},i}$ is the critical density (i.e. the density corresponding to the maximum flow in the fundamental diagram). An explicit lower bound ($v_{\min}$) is imposed for the mean speed in (2) in order to avoid unrealistically low or even negative speed predictions that are undesirable for identification purposes.

An extra term is added to the speed Eq. (2) if there is an on-ramp in link $i$ in order to account for the speed drop caused by merging phenomena:

$$-\frac{\delta_i T q_{\mathrm{r},i}(k) v_i(k)}{L_i \lambda_i (\rho_i(k) + K_i)} \tag{4}$$

where $\delta_i$ is a model parameter.

In order to complete the model, the following equation defines the flow that enters from an uncontrolled on-ramp or from the mainline origin:

$$q_{\mathrm{r},i}(k) = \min\left(C_{\mathrm{r},i},\ D_i(k) + \frac{w_i(k)}{T},\ C_{\mathrm{r},i}\frac{\rho_{\mathrm{m},i} - \rho_i(k)}{\rho_{\mathrm{m},i} - \rho_{\mathrm{c},i}}\right) \tag{5}$$

where $\rho_{\mathrm{m},i}$ and $C_{\mathrm{r},i}$ are model parameters, $D_i(k)$ is the demand of the on-ramp connected to link $i$ or of the mainline origin connected to link 1, and $w_i(k)$ is the queue length on ramp $i$ or on the mainline origin, the dynamics of which are given by:

$$w_i(k+1) = w_i(k) + T(D_i(k) - q_{\mathrm{r},i}(k)) \tag{6}$$

The downstream density of the last link and the upstream speed of the first link are considered as inputs of the system and are

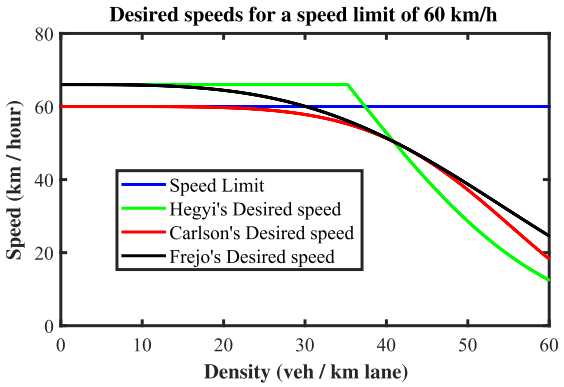


**Fig. 1.** Desired speeds for $v_{f,i} = 120$ km/h, $\rho_{c,i} = 30$ veh/(km lane), $a_i = 2.5$, $V_{c,i}(k) = 60$ km/h, $\alpha_i = 0.1$, $A_i = 0.8$, $E_i = 3$ (for Carlson's model), $A_i = 0.889$, and $E_i = 1.78$ (for Frejo's model).

taken from real data (or estimated based on the data available) or defined with boundary conditions.

## 3. Macroscopic VSL modeling

### 3.1. VSL model of Hegyi et al.

In the related literature, two main ways of including the effects of VSLs in METANET have been considered. The first one was proposed by Hegyi et al. (2004) in 2004. In this model, VSLs are included in the model by modifying the desired speed equation. When a VSL is applied, the desired speed is computed by taking the minimum of two quantities: the speed based on the prevailing traffic conditions, and the speed caused by the VSL (affected by a compliance term):

$$V_i(k) = \min\left(v_{f,i} e^{-\frac{1}{a_i}\left(\frac{\rho_i(k)}{\rho_{c,i}}\right)^{a_i}}, (1+\alpha_i)V_{c,i}(k)\right) \tag{7}$$

where $V_{c,i}(k)$ is the value of the speed limit on link $i$, and $\alpha_i$ is a model parameter that reflects the driver compliance.

An example of the desired speed of a link obtained under the influence of a VSL can be seen in Fig. 1. The corresponding Fundamental Diagram (FD), the steady-state relation between flow and density, can be seen in Fig. 2.

Assuming that the parameters of the original METANET model ($v_{f,i}$, $\rho_{c,i}$, $a_i$...) are known, the effect of the application of VSLs on the three characteristic parameters of the FD (critical density $\rho^*_{c,i}$, free flow speed $v^*_{f,i}$ and capacity $q^{max}_{V_{c,i}}$) according to Hegyi's model is the following:

- **VSL-induced free-flow speed:** The new free-flow speed, influenced by a VSL, is given by:

$$v^*_{f,i}(k) = \min((1+\alpha_i)V_{c,i}(k), v_{f,i}) \tag{8}$$

  Compliance can be adjusted by parameter $\alpha$ and, therefore, for a given value of $v_{f,i}$ and $V_{c,i}(k)$, any value (between $V_{c,i}(k)$ and $v_{f,i}$) for the VSL-induced free flow speed can be set according to the measurements.
- **VSL-induced critical density:** The new critical density is computed by intersecting the original FD with the speed line given by

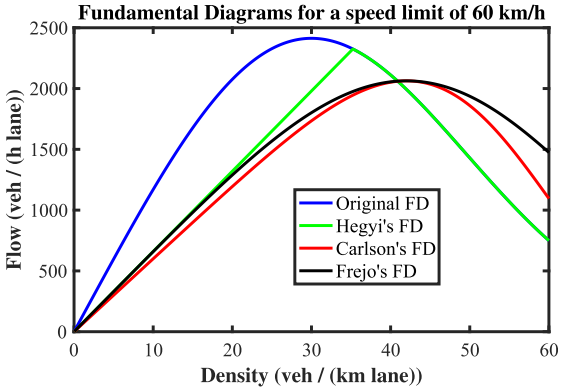


**Fig. 2.** FD with the same parameters as Fig. 1.

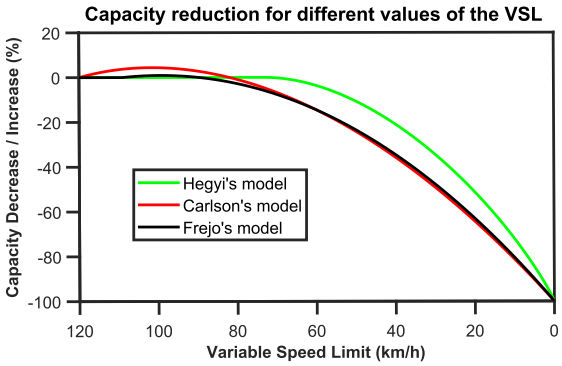


**Fig. 3.** Capacity reduction (%) with respect to original FD with the same parameters as Fig. 1.

the VSL-induced free flow speed or by taking the original critical density if the intersection is on the uncongested part of the FD:

$$\rho^*_{c,i}(k) = \rho_{c,i}\max\left(\left(-a_i \ln\frac{(1+\alpha_i)V_{c,i}(k)}{v_{f,i}}\right)^{1/a_i}, 1\right) \tag{9}$$

For a given compliance and original FD, the VSL-induced critical density cannot be adjusted (i.e. calibrated according to real data).

- **VSL-induced capacity:**Equivalently, the capacity induced by the VSL cannot be adjusted and its value is computed by:

$$q^{max}_{V_{c,i}}(k) = \min\left(\rho^*_{c,i}(k)v^*_{f,i}(k), \rho_{c,i}v_{f,i}e^{\frac{-1}{a_i}}\right) \tag{10}$$

The obtained capacity reduction (with respect to the capacity corresponding to a speed limit of 120 km/h) as a function of the value of the speed limit is shown in Fig. 3. As can be seen in the figure, the capacity reduction is usually relatively small or even zero for high and intermediate speed limits. For example, for the FD shown in Fig. 2, the capacity is reduced only by a 3.65% with the VSL being half (60 km/h) of the nominal speed limit (120 km/h).

### 3.2. VSL model of Carlson et al.

The second model that is commonly used in the literature was proposed by Papamichail et al. (2008) in 2008 and it has been mainly used by Carlson et al. (2010, 2011). In this model, FD parameters are modified to incorporate the influence of the VSLs. The speed ratio $b_i(k)$ (defined between 0 and 1) is used instead of the implemented value of the speed limit $V_{c,i}(k)$:

$$V_i(k) = v^*_{f,i}(k)e^{-\frac{1}{a_i^*(k)}\left(\frac{\rho_i(k)}{\rho^*_{c,i}(k)}\right)^{a_i^*(k)}} \tag{11}$$

$$b_i(k) = \frac{V_{c,i}(k)}{V^{\max}_{c,i}(k)}$$
$$v^*_{f,i}(k) = v_{f,i}b_i(k)$$
$$\rho^*_{c,i}(k) = \rho_{c,i}(1 + A_i(1 - b_i(k)))$$
$$a_i^*(k) = a_i(E_i - (E_i - 1)b_i(k))$$

It has to be pointed out that $b_i(k)$ is defined in two ways in Carlson et al. (2010) (and other later references): "$b_i(k)$ is equal to the VSL-induced $v^*_{f,i}$ divided by the non-VSL $v_{f,i}$ or approximately equal to the displayed VSL divided by the legal speed limit without VSL." The first definition cannot be used for calibration because the actual implemented input is the speed limit $V_{c,i}(k)$ and $v_{f,i}$ and $v^*_{f,i}$ are unknown before the calibration. Therefore, in this paper the second definition is considered as shown in (11). An example of the desired speed and FD obtained with this model can be seen in Figs. 1 and 2.

According to Carlson's model, the three characteristic parameters of the FD change as follows:

- **VSL-induced free-flow speed:** Since compliance is not included, it is assumed that the VSL-induced free-flow speed is equal to the value of the corresponding speed limit (i.e. for steady states with low densities, the mean speed of a link will be equal the current VSL value in the corresponding link).
- **VSL-induced critical density:** The critical density induced by a VSL can be easily adjusted in order to approach real data by changing the parameter $A_i$ as shown in Eq. (11).
- **VSL-induced capacity:** The capacity induced by a VSL can be calibrated by adjusting the parameters $E_i$ and $A_i$:

$$q^{max}_{V_{c,i}}(k) = \rho^*_{c,i}(k)v^*_{f,i}(k)e^{\frac{-1}{a_i^*(k)}} \tag{12}$$

The obtained capacity reduction is shown in Fig. 3. As can be seen in the figure, for the given values of the model parameters, the capacity is slightly increased for high values of the VSL. On the other hand, for intermediate and low values of the VSL, there is a significant capacity reduction (that can be adjusted by using (11) and (12)).

### 3.3. New proposed model

As previously explained, Hegyi's model can be adapted for different VSL-induced free flow speeds, but it lacks the capability of modeling different capacity reductions and critical densities due to the effects of VSLs. On the other hand, Carlson's model is able to model different VSL-induced capacities and critical densities, but it does not consider different levels of compliance.

In this paper, a new model is proposed combining the advantages of both approaches. The effect of a VSL is modeled by modifying the FD parameters including a calibration parameter for each equation ($\alpha_i$ for $v_{f,i}$, $A_i$ for $\rho_{c,i}$, and $E_i$ for $a_i$):

$$V_i(k) = v^*_{f,i}(k)e^{-\frac{1}{a_i^*(k)}\left(\frac{\rho_i(k)}{\rho^*_{c,i}(k)}\right)^{a_i^*(k)}} \tag{13}$$

$$b_i^r(k) = \min\left(\frac{V_{c,i}(k)}{V_{c,i}^{\max}(k)}(1+\alpha_i),\ 1\right)$$
$$v^*_{f,i}(k) = \min(V_{c,i}^{\max}(k)b_i^r(k),\ v_{f,i})$$
$$\rho^*_{c,i}(k) = \rho_{c,i}(1 + A_i(1 - b_i^r(k)))$$
$$a_i^*(k) = a_i(E_i - (E_i - 1)b_i^r(k))$$

Moreover, in contrast to Carlson's model, the VSL-induced free-flow speed depends on the maximum value of the speed limit and does not depend on the free-flow speed without VSL. This definition is more realistic for links that have a maximum value for the VSL that is larger than the maximum free-flow speed. For example, for a link with full compliance, a maximum speed limit of 120 km/h and a free-flow speed of 100 km/h, the VSL-induced free-flow speed for a speed limit of 60 km/h should be 60 km/h (and not 50 km/h).

An example of the desired speed and FD obtained with the proposed model can be seen in Figs. 1 and 2. According to the model, the three characteristics parameters of the FD changes as follows:

- **VSL-induced free-flow speed:** Compliance can be adjusted by the parameter $\alpha$; hence the VSL-induced free flow speed can be freely set according to real data as shown in (13). It is noted that compliance is also affecting the VSL-induced critical density and capacity. This allows to adapt an already calibrated model if the compliance changes (e.g. if the speed limit compliance is enforced by fines or other measures).
  In Fig. 4, the FDs and the desired speeds obtained for different values of the compliance $\alpha$ are shown. The figure is equivalent to the one that would be obtained for different values of the VSL having the same compliance. It can be seen that, as expected from real traffic, the influence of the speed limits (and their compliance) is very low when the system is considerably congested.
- **VSL-induced critical density:** The critical density induced by a VSL can be adjusted in order to approximate real data by changing the parameter $A_i$ as shown in (13).
- **VSL-induced capacity:** The VSL-induced capacity can be also adjusted in order to fit measurements by using the parameters $E_i$ and $A_i$:

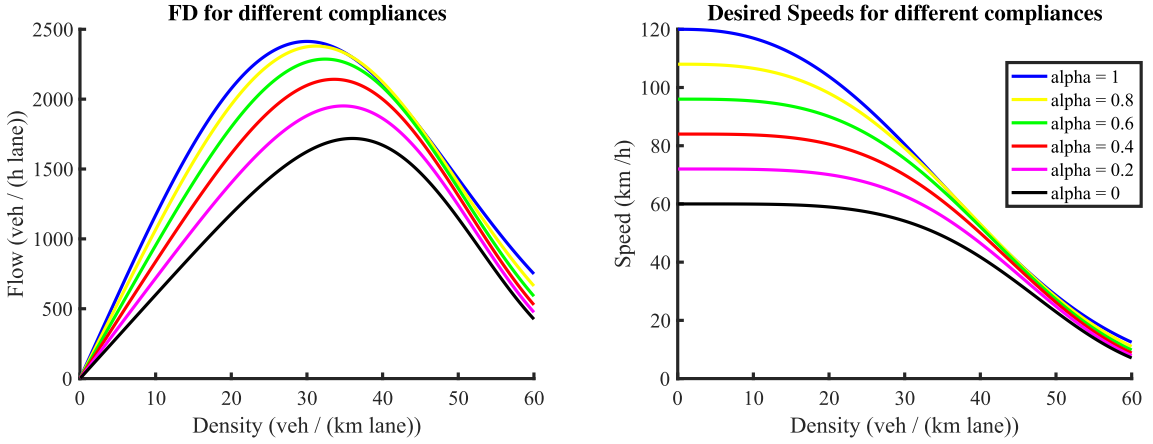


**Fig. 4.** FD and desired speed for different levels of compliance using Frejo's model with $v_{f,i} = 120$ km/h, $\rho_{c,i} = 30$ veh/(km lane), $a_i = 2.5$, $V_{c,i}(k) = 60$ km/h, $A_i = 0.4$, and $E_i = 2.5$.

$$q_{V_{c,i}}^{\max}(k) = \rho_{c,i}^{*}(k) v_{f,i}^{*}(k) e^{\frac{-1}{a_i^{*}(k)}} \tag{14}$$

The obtained capacity reduction is shown in Fig. 3. In this case, for intermediate and low values of the VSL, there is a significant capacity reduction (that can be adjusted by using (13) and (14)). For high values of the VSLs, the capacity is not substantially affected.

In summary of effects on the FDs of the considered model, Hegyi's model can be adapted for different VSL-induced free flow speeds, but it lacks the capability of modeling different VSL-induced capacity reductions and critical densities while Carlson's model is able to model different VSL-induced capacities and critical densities, but it does not consider different levels of compliance. On the other hand, the newly proposed model can be adapted for different VSL-induced free-flow speeds, capacities, and critical densities.

The main disadvantage of the proposed model is that 3 parameters have to be adjusted for each link (while only one is necessary for Hegyi's model and two for Carlson's model). The additional parameter is not going to affect substantially simulation times or optimization computational loads. However, the calibration effort will be accordingly increased.

From now on, in order to simplify the comparison with the other two approaches, the newly proposed model will be called Frejo's model.

Finally, it should be noted that, using the models considered in this paper, the fundamental diagram can be modified even if a speed limit is above the critical speed or if the actual speed of traffic is lower than the VSL in force. The data set available in this work does not allow to refute or confirm this behavior but this is an interesting topic for future works.

## 4. Considered network

The calibration data used in this paper comes from the application of the SPECIALIST algorithm in a part of the Dutch A12 freeway (Hegyi and Hoogendoorn, 2010). The considered stretch is located between the connection with the N11 at Bodegraven (which is not included in this study) up to Harmelen. As can be seen on the schematic representation of the freeway stretch in Fig. 5, the stretch has three lanes, 23 links and a length of 14.01 km.

The stretch is equipped with variable message signs, that display the current VSL, located at the beginning of each link. Under each gantry there are also double-loop detectors (one pair for each lane), measuring speeds and flows.

The data set used includes speed and flow measurements with a sampling time of 10 s (computed as a moving average of the last minute) collected during six months (from September 2009 to February 2010). The data set also includes the speed limit values that have been shown on the variable message signs. The default speed limit is 120 km/h and the possible values of displayed variable speed limits are 50, 60, 70, 80, 90, 100, and 120 km/h.

The aggregated flow of each link is directly taken from the corresponding loop detector at the beginning of the link while the aggregated speed is the arithmetic mean of the speeds measured in the loop detectors at the beginning and at the end of each link. In a future work, the harmonic speed may be used (instead of the aggregated speed) in order to increase consistency when relating flow and density.

The stretch includes two on-ramps and two off-ramps (at Nieuwerbrug, and at Woerden). The on-ramp demands and the split ratios are estimated from mainline data (by subtracting exponentially smoothed averages of the mainline flow upstream and downstream of the ramps).

The network does not show recurrent congestion from a bottleneck. The most common traffic jams appearing on the freeway are shock waves originating from further downstream of the freeway stretch (D3). For some days, the freeway stretch also shows non-recurrent congestion caused by bottlenecks and abnormally high demands. For example, a bottleneck on link 15 is observed during some periods. Moreover, within the data set, some traffic jams are observed, which are caused by incidents such as accidents or lane closures.

When a shock wave is considered to be resolvable by the SPECIALIST algorithm, the VSLs are activated upstream of the jam. In some cases, the algorithm is able to successfully resolve the traffic jam, while in other cases the congestion remains or even a new traffic jam is created upstream of the links where the VSLs were applied.

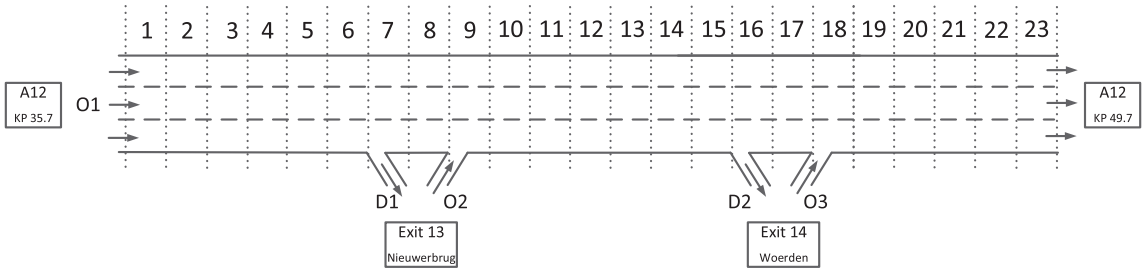


**Fig. 5.** Schematic representation of the considered A12 stretch. The 23 links have a length of [630, 530, 530, 535, 600, 595, 480, 800, 725, 700, 700, 725, 656, 600, 600, 414, 655, 525, 494, 616, 665, 635, 600] m, respectively.

Unfortunately, the data set does not include speed and flow data for a wide range of density levels for every speed limit analyzed. Therefore, many detectors will not be used for the analysis of the effects of VSLs on capacity and critical density (Section 5) and/or for modeling the effects of VSL on uncongested traffic (Section 6).

In order to analyze the effects of VSLs, the following considerations have to be taken into account:

- The speed limits of 50 and 70 km/h, corresponding to the application of a queue tail warning system (called Automatic Incident Detection or AID), are only switched on if the traffic is already congested: If the speed of a link drops below a predefined threshold (usually around 35 km/h), a 50 km/h speed limit is displayed at the corresponding link, and a 70 km/h speed limit is displayed at the upstream link.
- The speed limit of 100 km/h is switched on depending on weather conditions (which implies a change in the values of the model parameters).
- The speed limit of 60 km/h corresponds to the SPECIALIST algorithm (usually applied on uncongested links).

## 5. VSL-induced capacity and critical density

Previous references have analyzed the potential increase (or decrease) of the critical density of a link affected by a VSL. The conclusion for the majority of the references (Papageorgiou et al., 2008; Soriguera et al., 2017; Soriguera et al., 2016; Smulders, 1990; van den Hoogen and Smulders, 1994; Zackor, 1972) is that the critical density is increased when speed limits are decreased.

On the other hand, different conclusions have been drawn about the potential reduction (or increase) of the capacity of a link affected by a VSL:

- Pioneer research (Zackor, 1972), using speed limits of 80 km/h, suggests a capacity increase due to the effect of VSLs.
- Later references (Smulders, 1990; van den Hoogen and Smulders, 1994), using speed limits of 90 and 70 km/h, conclude that VSLs do not increase capacity significantly.
- In (Knoop et al., 2010; Duret et al., 2012; Heydecker and Addison, 2011), using speed limits of 60 km/h, 110 km/h, and 40, 50, 60 mph (64.4, 80.5, 96.6 km/h), respectively, an increase in the utilization of the shoulder lane is observed without clear conclusions about aggregated capacity.
- In Papageorgiou et al. (2008) and Soriguera et al. (2017), using speed limits of 40, 50, 60 mph (64.4, 80.5, 96.6 km/h), and 40 km/h, respectively, a slight capacity reduction is observed but no clear conclusions about capacity decrease/increase are drawn.
- In Soriguera et al. (2016), a higher capacity reduction (around 15%) is observed due to the application of low VSLs (50 km/h)

When analyzing the capacity of a link under different speed limits, the following considerations should be taken into account:

- The analyzed link must be an active bottleneck of a traffic jam (if not recurrent, at least for a few different days or hours).
- It is necessary to have data with two different speed limits at the time that the considered bottleneck reaches capacity (i.e. a speed limit that is only applied for uncongested or already congested links does not allow to estimate VSL-induced capacity).
- It is preferable to use data with constant speed limits (while reaching congestion) in order to avoid dynamic effects that may hinder a proper capacity estimation.

With the exception of the study in Soriguera et al. (2016), the research works previously published (Zackor, 1972; Smulders, 1990; van den Hoogen and Smulders, 1994; Papageorgiou et al., 2008; Soriguera et al., 2017) do not completely fulfil these requirements for a proper capacity estimation.

Within the A12 data set considered in this study only one link fulfills the three mentioned conditions: A bottleneck (on kilometer point 44,7) that has different (but constant during long periods of time) values for the VSLs while reaching congestion (Link 15 for speed limits 120 km/h and 90 km/h).

In order to perform a fair analysis, only the days for which both speed limits are used are considered. Moreover, the days with a much lower free flow speed during long periods of the day (due to weather conditions) are not used. As a result, 34 days have been considered for this study.

Furthermore, in order to only consider congestion created by the own link (for which capacity can be estimated), the traffic jams coming from downstream links are not considered. This is achieved by taking away the measurement for which link 16 is congested, using a speed threshold ($v_{16}(k) < 80$ km/h).

In Fig. 6 the FD measurements obtained, after removing the non-useful points using the previously explained considerations, are shown. By inspection of the data, it can be seen that for both 90 km/h and 120 km/h there are some points that can be used to estimate capacity (because the slopes of the point clouds are strongly decreasing around densities of 27 or 28 veh/(km lane) and because the flows corresponding to higher densities are smaller than the capacity and have sparser distributions). Moreover, it can be seen that for $V_{c,i}(k) = 120$ km/h there are many points with higher flows (around the critical density) than the flows obtained with $V_{c,i}(k) = 90$ km/h (also around critical density).

If the point clouds are approximated, a capacity of 2418 veh/(h lane) and a critical density of 27 veh/(km lane) are obtained with $V_{c,i}(k) = 120$ km/h while a capacity of 2290 veh/(h lane) and a critical density of 28 veh/(h lane) is obtained with $V_{c,i}(k) = 90$ km/h.

Even through this capacity reduction is relativity low (around 5%), it is expected that the reduction will be higher for lower speed limits (as predicted by the FDs in Fig. 4). The critical density increase is even smaller (around 4%) but, again, higher critical densities

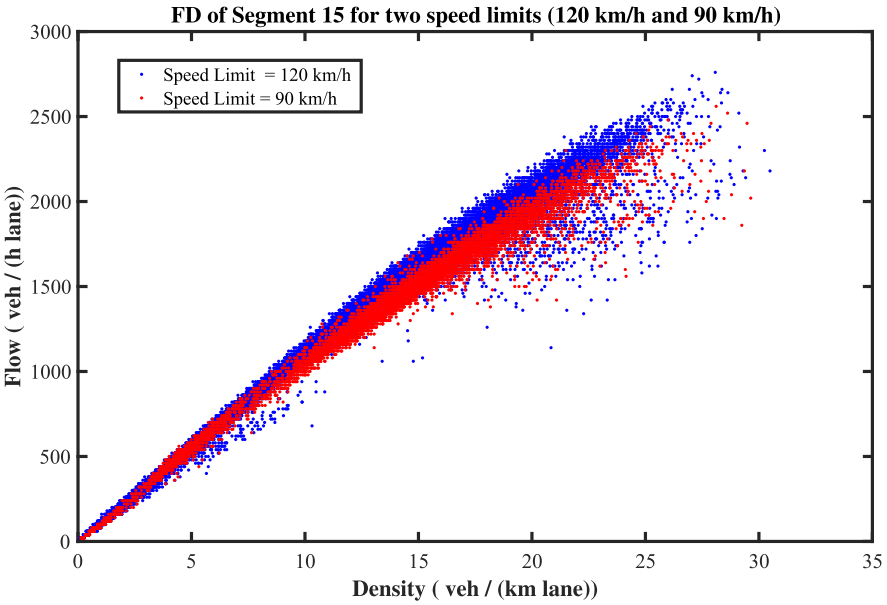


**Fig. 6.** Traffic data for Link 15 with $V_{c,i}(k) = 120$ km/h (blue) and $V_{c,i}(k) = 90$ km/h (red). (For interpretation of the references to colour in this figure legend, the reader is referred to the web version of this article.)

are expected for lower speed limits. However, it has to be pointed out that the validation of the model for 90 km/h does not necessarily imply the adequacy of the model for lower speed limits.

In Fig. 7, the FDs of the three VSL models presented in Section 3 are manually calibrated in order to approximate the measurements obtained with $V_{c,i}(k) = 90$ km/h based on a nominal FD calibrated for the data measured with $V_{c,i}(k) = 120$ km/h.

Firstly, the free-flow speed has been found by drawing the straight line that best approximates the FD data cloud for low densities. Based on this free-flow speed, the compliance parameter is determined. Subsequently, visual curve fitting is done based on the FD data cloud. Then, the maximum of the resulting curve is determined in order to obtain an estimate of the capacity and the critical density.

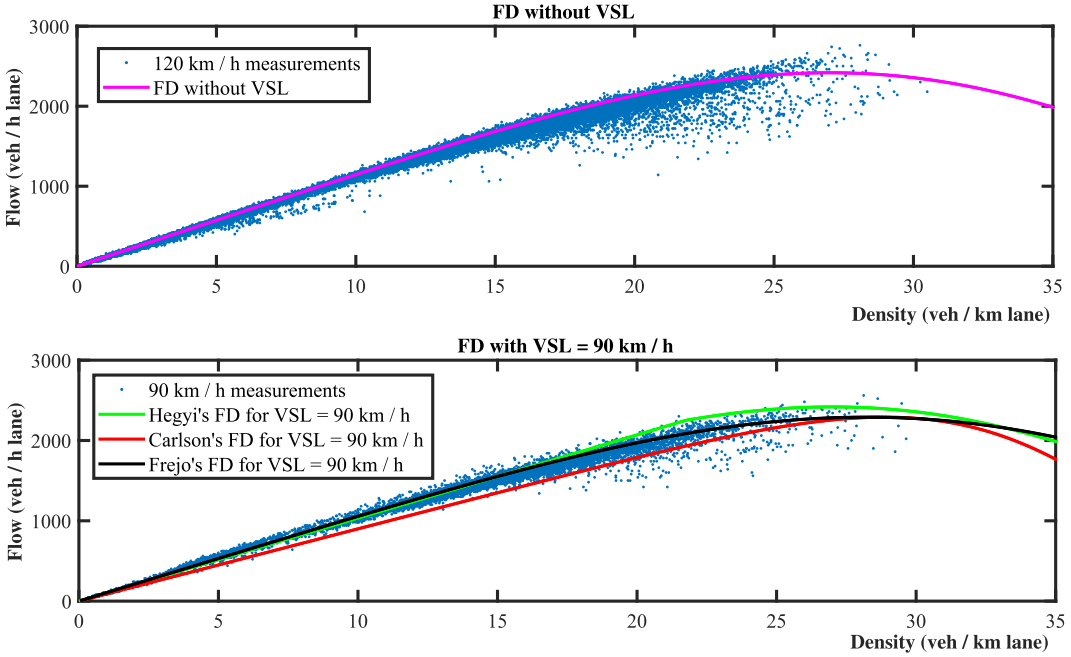


**Fig. 7.** Estimated FDs for Link 15 with $v_{f,i} = 115$ km/h, $\rho_{c,i} = 27$ veh/(km lane), $a_i = 4$, $V_{c,i}(k) = 90$ km/h, $\alpha_i = 0.15$ (for Hegyi's model), $A_i = 0.4245$ and $E_i = 5.5$ (for Carlson's model), and $\alpha_i = 0.18$, $A_i = 0.388$ and $E_i = 0.4$ (for Frejo's model).

**Table 1**
Modeled effects of VSL on critical density and capacity on Link 15.

| | No-VSL | Hegyi's | Carlson's | Frejo's |
|---|---|---|---|---|
| Capacity ($\frac{veh}{hlane}$) | 2418.2 | 2418.2 | 2290 | 2290 |
| Critical Density ($\frac{veh}{kmlane}$) | 27 | 27 | 29.86 | 28.20 |
| Critical Speed ($\frac{km}{h}$) | 89.56 | 89.56 | 76.69 | 81.21 |

Using the obtained capacity and critical density, parameters $E_i$ and $A_i$ of Carlson's and Frejo's models can be computed using (11)–(14). However, the VSL-induced critical densities for Carlson's and Frejo's models (29.86 veh/(km lane) and 28.20 veh/(km lane), respectively) have been set to a slightly higher value than the one previously identified for the original point clouds (28 veh/(h lane)) in order to avoid very low values of the parameter $E_i$, which would create unrealistic estimations for lower speed limits. If the value of the parameters of the VSL models were obtained by optimizing a dynamic traffic flow model (as in Section 7), this increase of the critical density would also appear in order to match FD data.

On the other hand, as explained in Section 3, Hegyi's model cannot be calibrated for capacity reductions different from the ones resulting from the model. Moreover, for high speed limits (like 90 km/h) the capacity is not reduced at all. In fact, as can be seen in the figure, the capacity and critical density given by Hegyi's model for the data analyzed are the same as for the original FD: 2418.2 veh/h lane, and 27 veh/(km lane).

The capacities and the critical densities obtained for each model are shown in Table 1.

According to the results in this section, the following conclusions may be drawn:

- As stated in previous references, the critical density of a link is increased by decreasing the corresponding VSL. This allows to store more vehicles (without reaching congestion) in a link upstream of a traffic jam and, therefore, to apply a VSL control algorithm for traffic efficiency improvement as the ones proposed in (Carlson et al., 2011; Hegyi et al., 2008; Frejo et al., 2014).
- At least for some scenarios, the capacity of a link is decreased due to a reduction of the corresponding VSL. This allows to increase the benefits of the previously cited VSL control algorithms for traffic efficiency improvement (as explained in Carlson et al. (2010)).
- The lack of capability of Hegyi's model to be calibrated for different VSL-induced capacities and critical densities may be one of its main drawbacks (especially when this model is used to predict the traffic behavior for freeways where VSLs are applied to congested links reaching capacity or when the VSL-induced capacity reduction is used to decrease the flow entering a downstream bottleneck).
- On the other hand, Carlson's and Frejo's models may be adapted to match any VSL-induced critical density and any VSL-induced capacity for each link. Therefore, they may deliver a better prediction for scenarios where VSLs are applied to links reaching capacity.

## 6. Modeling the effects of VSL on uncongested traffic

For freeway traffic control using VSLs metering capabilities, the speed limits are generally applied on uncongested links upstream of a bottleneck that has reached (or is going to reach soon) the critical density (Carlson et al., 2011; Hegyi et al., 2008; Frejo et al., 2014). Moreover, when a link is already congested due to a downstream bottleneck, the potential improvement in the traffic performance if a VSL is applied on that link is not significant (or even no improvement at all can be achieved). Therefore, when using macroscopic models in order to compute or test VSL control algorithms, the most important aspect is how the speed of an uncongested link evolves when a speed limit is applied.

This section analyzes how each considered model predicts the response of the traffic when speed limits are applied on uncongested links and how these predictions match with the real data available from the A12 freeway.

Fig. 8 shows the flow and speed measurements for three different links obtained when a speed limit of 60 km/h is applied. In these figures, data were used from all the days for which SPECIALIST was applied. The measurements obtained during the first two minutes after the application of the 60 km/h speed limit have been removed in order to remove transient effects of the application of the VSL.

In the three links shown, the same shapes of the point clouds can be observed. For other links, the measurements are similar. Analyzing the measurements, the following conclusions can be drawn:

- For low densities, the compliance is very low. For example, it can be seen that the measured speeds are around 90 km/h when the densities are lower than 15 veh/km lane. It has to be pointed out that the compliance may be increased by an enforcement measure, in which case the speed of the drivers will approach the speed limit. However, even with an enforcement measure, only in a few scenarios the real traffic is going to have full compliance. For example, in some circumstances the drivers may drive within the fine tolerance zone which reaches usually 5% or 10% higher that the actual speed limit). Therefore, it can be concluded that including the driver compliance in a VSL model is quite beneficial in order to increase model accuracy.
- When densities are increased (even being lower than the critical density), the desired speeds start to decrease substantially. For example, it can be seen in the figures that the measured speeds are around 70 km/h when the densities are about 25 veh/(km lane)

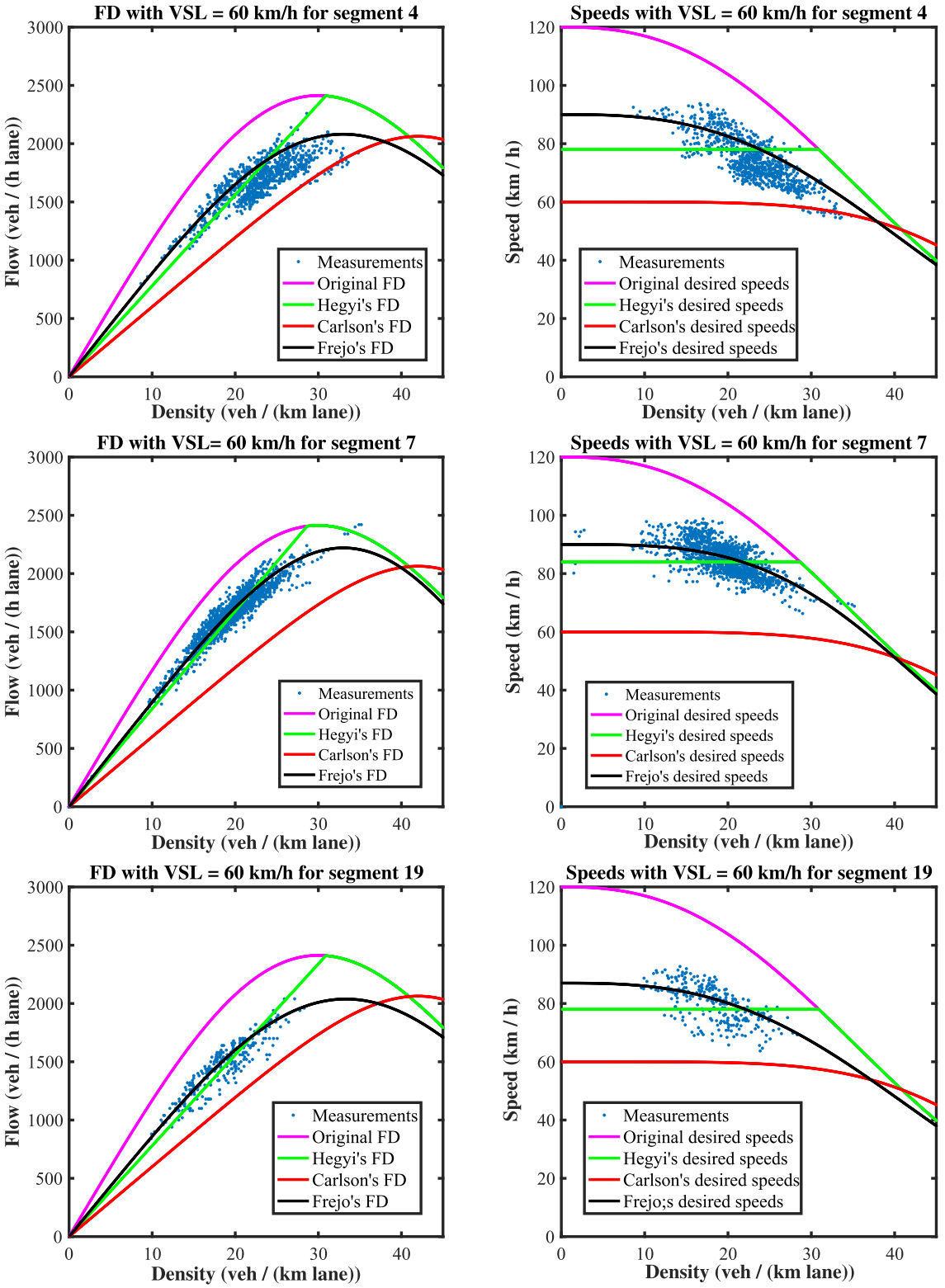


**Fig. 8.** FD diagrams and Desired Speeds for Links 4, 7 and 19 with $v_{f,i}$ = 120 km/h, $\rho_{c,i}$ = 30 veh/(km lane), $a_i$ = 2.5, $\alpha_i$ = 0.3 (for Hegyi's model), $E_i$ = 3, $A_i$ = 0.8 (for Carlson's model), $\alpha_i$ = 0.5, $E_i$ = 1.5, and $A_i$ = 0.4 (for Frejo's model).

(20 km/h less that the speed observed at low densities). Therefore, it can be concluded that the VSL-induced FD is not triangular for the uncongested part (equivalently to the FD without VSLs) and the use of an exponential equation increases the accuracy of the prediction.

The desired speeds and FDs obtained using each model are also shown in Fig. 8. The following conclusions can be drawn about the drawbacks of each model when predicting the effects of VSL on uncongested links:

- In order to properly model the VSL-induced free-flow speed, a high value of $\alpha_i$ (around 0.5 for A12 data) have to be used in some scenarios (especially when enforcement measures are not applied). Carlson's model considers that the VSL-induced free-flow speed is equal to the actual VSL so this model is not able to properly model this kind of response with such a low compliance. As previously explained, Carlson's model would be able to have a better VSL-induced free-flow speed if an enforcement measure is applied but, even in these cases, a value of $\alpha_i$ around 0.05 is expected after calibration.
- Carlson's and Frejo's models predict that the VSL-induced speeds decrease when densities increase because they use an exponential equation for the FD. Therefore, they are able to accurately approximate the behavior observed in the A12 data. On the other hand, using Hegyi's model the VSL-induced speeds are expected to have the same value for any density until they reach the speed given by the original FD (without VSLs). As a result, after calibration, the parameter $\alpha_i$ will probably take an intermediate value that predicts speeds lower than the real ones for low densities, but higher than the real ones for high, but uncongested, densities.

Combining the two conclusions stated above and analyzing the figures, it can be seen that Frejo's model is able to capture more accurately, and in a more general way, the effects of VSLs on uncongested links. This will allow to have a better, and more realistic, performance if a model-based VSL control algorithm is applied to an uncongested link in order to reduce the flow entering a traffic jam located downstream of the link where the VSL is applied.

## 7. Model calibration

In this section, calibration of the parameters of the three considered models is undertaken for the same data set: September 17, 2009 from 6:00 to 12:00. During this day, two traffic jams are created as can be seen on Fig. 9:

- Firstly, shortly before 7:00, congestion is created on Link 15 (9.4 km from the origin) probably due to the effect of the off-ramp. This congestion propagates upstream reaching the first considered link.
- Later, around 7:50, a new traffic jam is created on a bottleneck on Link 22 (13.4 km from the origin). This traffic jam also propagates downstream reaching the traffic jam created on Link 15 before it disappears.
- Congestion finishes around 9:15. Then, around 10:00, a new, but smaller, traffic jam is created also on Link 22.

The appearance of two bottlenecks during this day allows to obtain a better calibration of the model parameters than if other days were used (because for the majority of the days available in the data set the traffic jams appearing on the freeway are shock waves originating from further downstream of the freeway or traffic jams caused by incidents).

During the considered period, speed limits of 90, 70, 60, and 50 km/h are applied. As previously explained in Section 4, the speed limits of 70 km/h and 50 km/h (AID system) are used only when the system is already congested. Although the activation of the AID system is helping the model to estimate when the system is congested, these speed limits cannot be removed since they are indeed influencing traffic speed and flow. In order to perform a totally fair comparison, only periods of time when the AID system is not applied may be considered but this implies to consider only short uncongested periods of time and, thus, being unable to estimate capacities. In Section 9, short-term predictions are discussed to compare the behavior of the models when the SPECIALIST algorithm is applied.

The parameter estimation has been conducted using the software CALISTO (Spiliopoulou et al., 2014, 2017) (modified in order to include the models considered in this paper). CALISTO solves a nonlinear least-squares optimization problem minimizing the

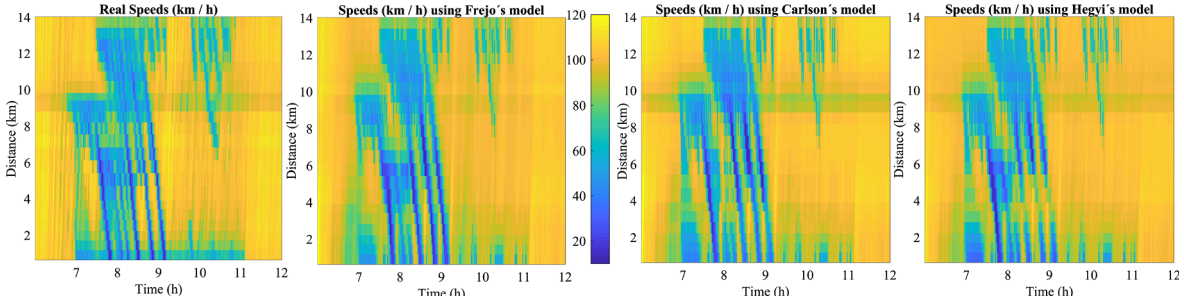


**Fig. 9.** Measured and estimated speed contour plots for September 17 (calibrated day).

**Table 2**
METANET parameters for Hegyi's model.

| $\tau_i$ | $\mu_i$ | $\delta_i$ | $\alpha_i$ | $K$ |
|---|---|---|---|---|
| 26. 20 s | 40. 49 $\frac{km^2}{h}$ | 1. 4·10$^{-7}$ | 0.2947 | 10 |

| | $a_i$ | $v_{f,i}$ | $\rho_{c,i}$ | $E_i$ | $A_i$ |
|---|---|---|---|---|---|
| FD 1 | 2. 31 | 111. 18 $\frac{km}{h}$ | 32. 63 $\frac{veh}{kmlane}$ | – | – |
| FD 2 | 3.41 | 108.2 $\frac{km}{h}$ | 29.38 $\frac{veh}{kmlane}$ | – | – |
| FD 3 | 3.51 | 112.7 $\frac{km}{h}$ | 25.85 $\frac{veh}{kmlane}$ | – | – |
| FD 4 | 3.01 | 103.8 $\frac{km}{h}$ | 34.76 $\frac{veh}{kmlane}$ | – | – |
| FD 5 | 3.54 | 105.2 $\frac{km}{h}$ | 34.62 $\frac{veh}{kmlane}$ | – | – |

discrepancy between the model predictions and the real traffic measurements by use of the following cost function:

$$J(p) = \sqrt{\frac{1}{N_t}\sum_{k=1}^{N_t}(\hat{y}(k) - \bar{y}(k,p))^2} \tag{15}$$

where $\hat{y}(k)$ is the measurement vector (including the speeds and flows measured for each link), $\bar{y}$ is the prediction vector (including the speeds and flows predicted for each link by the model), $N_t$ is the number of time steps, and $p$ is the vector including the parameters to be calibrated (i.e. FD and speed equation parameters).

The results presented correspond to the best obtained calibration after several runs with different initial values for the parameters of the models and two optimization algorithms (Nelder-Mead (Nelder and Mead, 1965) and a genetic algorithm (Goldberg, 1989)).

The network has been split in five groups of links considering a different set of FD parameters for each section (including parameters $E_i$ and $A_i$). The section grouping has been done heuristically based on the observed differences between the responses of each link. The first group includes Links 1, 2 and 3, the second group includes Links 5, 6, and 8, the third one includes Links 4, 7, 8, 9, 10, 11, 12, and 13, the forth group includes Links 14 and 15, and the last group includes links from 16 to 23. The parameters of the speed equation and the compliance parameter are considered equal for all the links. The parameters $K$ and $v_{min}$ are not calibrated and they are directly set as $K = 10$ veh/(km lane) and 7 km/h, respectively, because they are known, from previous METANET validations, to be of minor importance.

The parameters obtained for Hegyi's, Carlson's and, Frejo's models are shown in Tables 2–4, respectively. It can be seen that the parameters obtained for the three models are relatively similar with the most significant differences appearing in compliance parameter $\alpha_i$. Furthermore, the values of the parameters are of the same order of magnitude as the ones obtained for previous identifications of the METANET model despite the fact that the optimization used for the identification was not bounded. However, the values obtained for $\delta_i$ are really low implying that the speed decrease due to the merging phenomena is not relevant for this scenario.

The speed contour plots obtained with each model are shown in Fig. 9. In the plots, it can be seen that the predictions given by the three models are quite similar with a slightly better approximation to the original data obtained with Frejo's model. In fact, the three models are able to approximate the real data with high accuracy due to the activation of the AID system (as it helps to estimate speeds when the network is congested).

By way of example, the results for links 2 and 6, also including the implemented VSLs, are shown in Fig. 10. In the figure, it can be seen that the highest differences between the predictions of the models appears when the 60 km/h speed limit is applied (especially

**Table 3**
METANET parameters for Carlson's model.

| $\tau_i$ | $\mu_i$ | $\delta_i$ | $\alpha_i$ | $K$ |
|---|---|---|---|---|
| 32.04 s | 49.93 $\frac{km^2}{h}$ | 2.4·10$^{-7}$ | – | 10 |

| | $a_i$ | $v_{f,i}$ | $\rho_{c,i}$ | $E_i$ | $A_i$ |
|---|---|---|---|---|---|
| FD 1 | 1.68 | 117.6 $\frac{km}{h}$ | 35.21 $\frac{veh}{kmlane}$ | 1.55 | 0.455 |
| FD 2 | 2.71 | 116.1 $\frac{km}{h}$ | 25.17 $\frac{veh}{kmlane}$ | 1.61 | 0.033 |
| FD 3 | 4.45 | 107.1 $\frac{km}{h}$ | 31.46 $\frac{veh}{kmlane}$ | 2.05 | 0.054 |
| FD 4 | 2.15 | 114.04 $\frac{km}{h}$ | 27.81 $\frac{veh}{kmlane}$ | 2.93 | 0.250 |
| FD 5 | 2.70 | 114.0 $\frac{km}{h}$ | 33.94 $\frac{veh}{kmlane}$ | 1.95 | 0.916 |

**Table 4**
METANET parameters for Frejo's model.

| $\tau_i$ | $\mu_i$ | $\delta_i$ | $\alpha_i$ | $K$ |
|---|---|---|---|---|
| 31.08 s | 50.11 $\frac{km^2}{h}$ | $1.9 \cdot 10^{-7}$ | 0.377 | 10 |

| | $a_i$ | $v_{f,i}$ | $\rho_{c,i}$ | $E_i$ | $A_i$ |
|---|---|---|---|---|---|
| FD 1 | 1.72 | 120.0 $\frac{km}{h}$ | 32.87 $\frac{veh}{kmlane}$ | 1.36 | 0.460 |
| FD 2 | 2.72 | 114.5 $\frac{km}{h}$ | 25.85 $\frac{veh}{kmlane}$ | 1.54 | 0.033 |
| FD 3 | 3.89 | 105.8 $\frac{km}{h}$ | 27.4 $\frac{veh}{kmlane}$ | 2.05 | 0.055 |
| FD 4 | 2.16 | 113.6 $\frac{km}{h}$ | 27.81 $\frac{veh}{kmlane}$ | 2.87 | 0.245 |
| FD 5 | 2.81 | 111.4 $\frac{km}{h}$ | 28.56 $\frac{veh}{kmlane}$ | 1.77 | 0.903 |

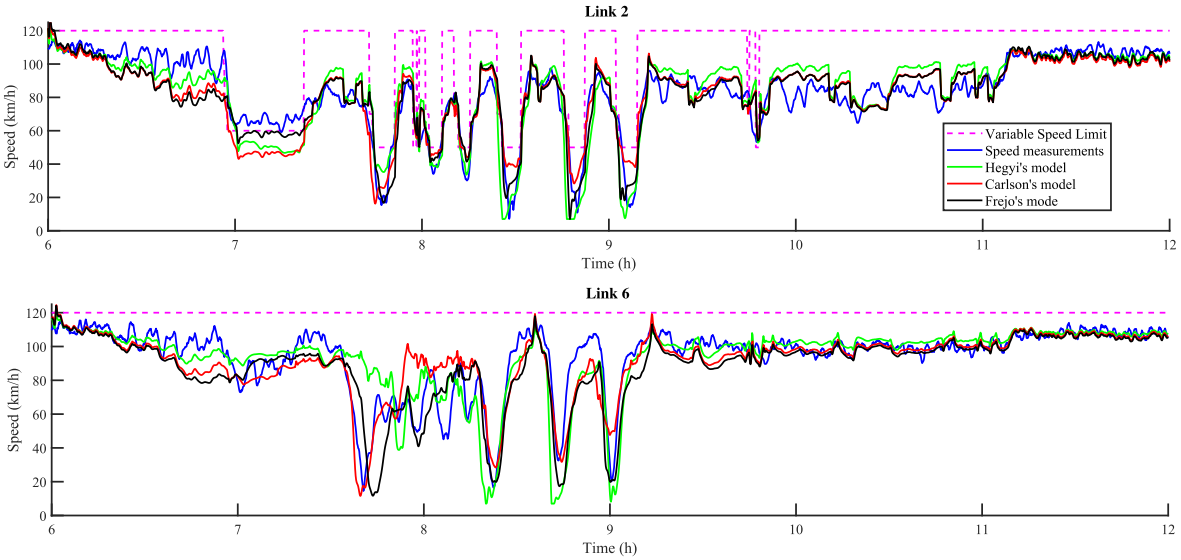


**Fig. 10.** Speeds for long-term simulation for September 17 (Links 2 and 6): Measurements (blue), VSL (magenta), Carlson's model (red), Hegyi's model (green) and Frejo's model (black). (For interpretation of the references to colour in this figure legend, the reader is referred to the web version of this article.)

on Link 2 between 6:55 and 7:23 AM) and for Link 6 between 7:40 and 7:50 AM (for which the AID system is not activated).

In Fig. 11, some details of the different predictions obtained with each model are shown. In the left figure, it can be seen that the speed predicted for Carlson's model (when the SPECIALIST algorithm is applied) is lower than the one obtained with the other two models. On the other hand, the speed predicted by Frejo's model is the closest to the real measurements. Different predictions can also be observed even for segments without a VSL, like the one on the right plot of Fig. 11, due to the variations in the modeling of the

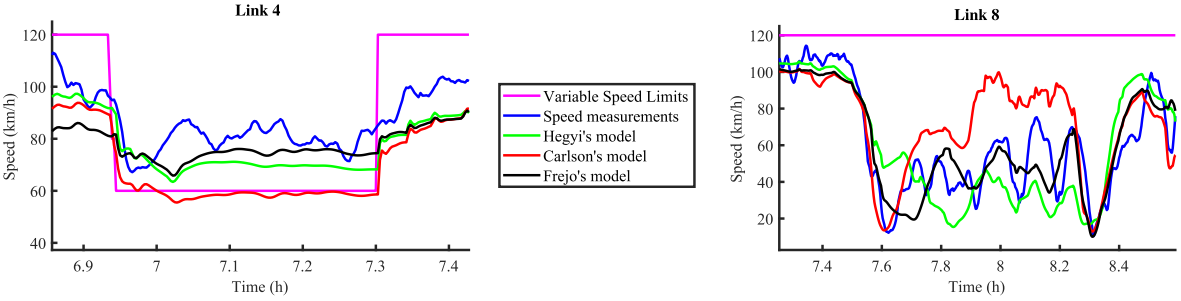


**Fig. 11.** Details of some observed differences between the considered models on two segments for September 17: Measurements (blue), VSL (magenta), Carlson's model (red), Hegyi's model (green) and Frejo's model (black). (For interpretation of the references to colour in this figure legend, the reader is referred to the web version of this article.)

**Table 5**
Mean relative speed errors.

| Day | Hegyi's | Carlson's | Frejo's |
|---|---|---|---|
| September 3 | 8.81% | 9.23% | 8.88% |
| September 15 | 12.84% | 13.41% | 10.72% |
| September 17 | 11.80% | 10.68% | 10.22% |
| September 18 | 8.32% | 8.08% | 8.02% |
| September 21 | 9.86% | 8.28% | 8.99% |
| September 28 | 6.50% | 6.02% | 7.2% |
| Day | Hegyi's | Carlson's | Frejo's |
| October 5 | 12.08% | 14.13% | 12.31% |
| October 9 | 12.75% | 14.34% | 13.41% |
| October 12 | 10.92% | 11.10% | 11.03% |
| October 13 | 13.18% | 14.31% | 13.83% |
| Mean | 9.82% | 10.03% | 9.57% |

effects of VSLs on upstream segments.

## 8. Validation for 6-h morning periods

In order to validate, using fresh data, the models identified in the previous section, the same time period (6:00–12:00) for ten days with significant congestion profiles have been used. It has to be pointed out that, due to the nonexistence of recurrent congestion, it is quite hard to obtain an accurate open-loop prediction (small disturbances can change the time when critical density is reached and, thus, substantially change the prediction). On the other hand, as it was previously explained, the 50 km/h and 70 km/h speed limits aid to improve the prediction since they are only activated when the system is already congested (so the prediction is not fully open-loop).

In order to compute the mean relative speed error, the following equation has been used:

$$\mathrm{MRE} = \sum_{k=1}^{N_t} \sum_{i=1}^{N_s} \frac{|\hat{v}_i(k) - \bar{v}_i(k)|}{\hat{v}_i N_t N_s} \tag{16}$$

where $\hat{v}_i(k)$ are the real speed measurements, $\bar{v}_i(k)$ are the estimated speeds, and $N_s$ is the number of links. The validation results can be seen in Table 5.

The three models considered are able to properly estimate speeds with a high accuracy (for such a long prediction horizon). A slightly better prediction (and so, a lower mean speed error) is obtained when using Frejo's model with a mean error of 9.57% for the 10 scenarios (versus 9.82% and 10.3% for Hegyi's and Carlson's models, respectively). In any case, it can be seen that the predictions obtained with the three models are quite similar. The reasons for this similarity are that:

- The 60 km/h and the 80 km/h speed limits are only applied during short periods of time (usually around 10 or 20 min) and only in a few links.
- For high densities, the responses of the three models are quite comparable because the congested FD does not change substantially with different values of the speed limits (as shown in Fig. 4) and because the anticipation and convection terms of the speed equation becomes more important for high densities (see Eq. (3)). Therefore, since the 50 km/h speed limits are applied when the system is already congested, they do not cause considerable differences between the models.

The speed contour plots obtained with each model for two validation days can be seen in Figs. 12 and 13. The first day shown (September 28) is an example of a day when a good prediction is obtained and also similar contour plots are obtained with each

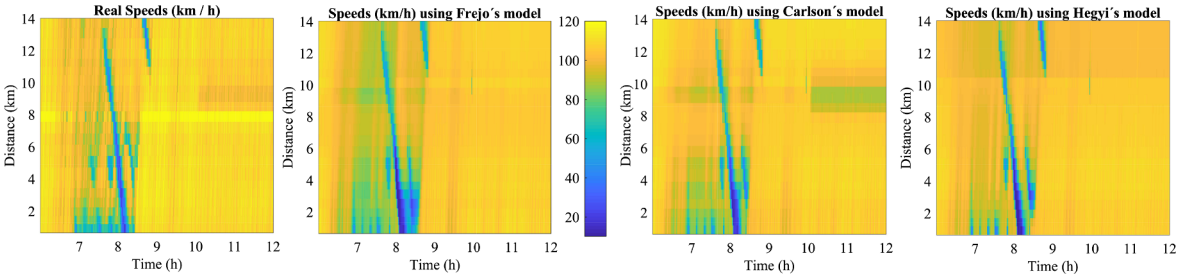


**Fig. 12.** Measured and estimated speed contour plots for September 28.

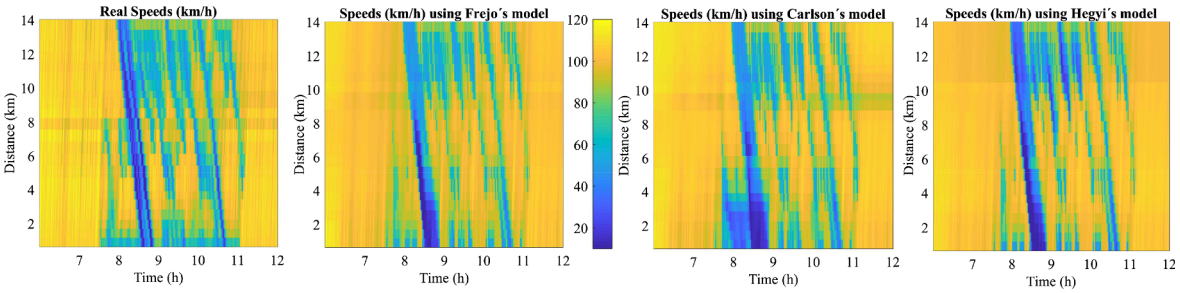


**Fig. 13.** Measured and estimated speed contour plots for October 9.

model. On the other hand, for the second day shown (October 9), disturbances lead to a bit less accurate predictions and higher differences between the speeds that are obtained with each model.

## 9. Validation for uncongested links

As explained in Section 6, one of the main differences between the considered models lays on the effect of VSLs when they are applied to uncongested links. Moreover, this is the most important aspect of a VSL model in terms of control design. Unfortunately, the effects of VSLs on uncongested segments are missing in the previous Sections 7 and 8 because the SPECIALIST algorithm is only applied during shorts periods of time and the rest of the activations of the VSLs are usually carried out when the freeway is already congested. On the other hand, this section is focused on the validation of the models for short periods of time during which the SPECIALIST algorithm was applied. This analysis allows to graphically visualize and numerically analyze the model differences explained in Section 6.

Firstly, the mean relative speed errors obtained for ten short scenarios for which VSL are applied to uncongested links are shown in Table 6. Eq. (16) has been used but, in this case, it only considers the links and the periods of time for which the 60 km/h speed limits were applied.

The results show that the speed errors obtained with Frejo's model are considerably smaller than the ones obtained with the other two models. Carlson's model has the largest errors because, as previously explained, it does not include compliance, which is a key aspect in order to model A12 data.

Subsequently, in order to visualize the numerical results of Table 6, two of the considered scenarios are graphically analyzed.

For the first plotted scenario, an activation of the SPECIALIST algorithm for links with very low densities is shown in Fig. 14 (December 18 from 00:00 to 00:30 AM). In this case, the capacity of the freeway is considerably reduced due to a non-recurrent event (probably an accident or a maintenance work that causes the closure of two lanes). In order to prevent the propagation of the created jam, SPECIALIST algorithm is applied upstream of the links affected by the capacity reduction. Since the simulation considered covers the period from 0:00 to 0:30 AM, the links for which SPECIALIST is applied (i.e. a 60 km/h speed limit is set) have a very low density at the time of the application (lower than 5 veh/ km lane).

The speeds measured for two significant links when the SPECIALIST algorithm is applied, and the corresponding predicted speeds, are shown in Fig. 15. In this case, since the densities are so low, the desired speeds given by each model are almost equivalent to the VSL-induced free-flow speeds. For the reason that the VSL compliance in this study is really low (as shown in Section 6), Carlson's model gives the worst prediction of the three models. On the other hand, Frejo's model is able to predict the VSL profiles with much more accuracy. Hegyi's model gives results that are slightly worse than Frejo's model because its compliance parameter $\alpha_i$ is smaller. This happens because, when the calibration is run, Hegyi's model needs to set a lower value for the compliance parameter $\alpha_i$ than the

**Table 6**
Mean relative speed errors when VSLs are applied on uncongested links.

| Day | Hegyi's | Carlson's | Frejo's |
|---|---|---|---|
| September 29 (8:00–8:30) | 17.46% | 35.22% | 16.83% |
| October 5 (7:00–7:30) | 11.64% | 28.09% | 8.77% |
| October 9 (7:30–8:00) | 13.64% | 35.12% | 10.66% |
| October 11 (8:30–9:00) | 11.26% | 26.22% | 5.97% |
| October 12 (15:30–16:30) | 19.44% | 37.34% | 11.04% |
| October 17 (8:00–8:30) | 9.72% | 24.88% | 4.94% |
| Day | Hegyi's | Carlson's | Frejo's |
| October 23 (9:30–9:00) | 9.83% | 27.98% | 8.41% |
| October 30 (8:00–8:30) | 11.86% | 27.33% | 9.87% |
| November 9 (14:30–15:00) | 9.54% | 27.54% | 6.83% |
| December 18 (0:00–0:30) | 13.96% | 31.07% | 9.58% |
| **Mean** | **12.84%** | **30. 08%** | **9. 29%** |

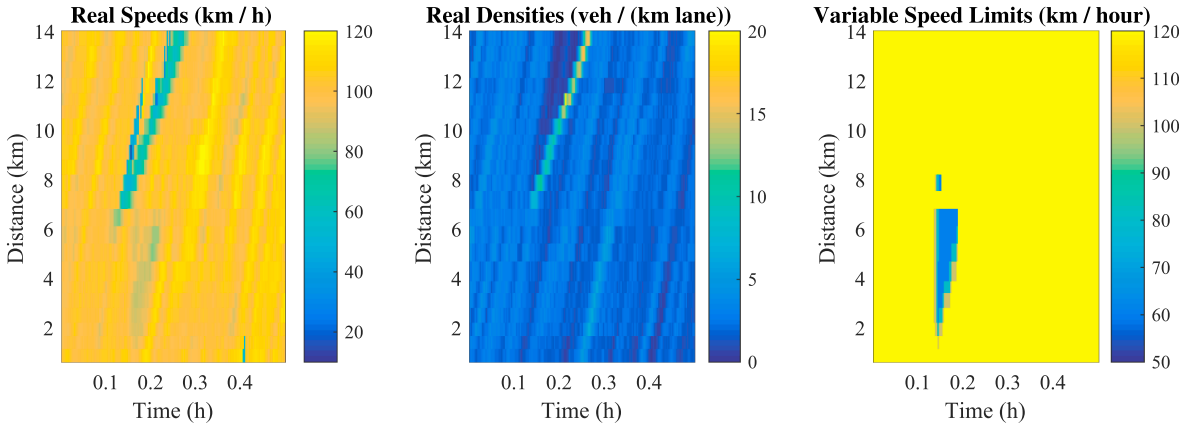


**Fig. 14.** Real speeds, densities and VSLs for December 18.

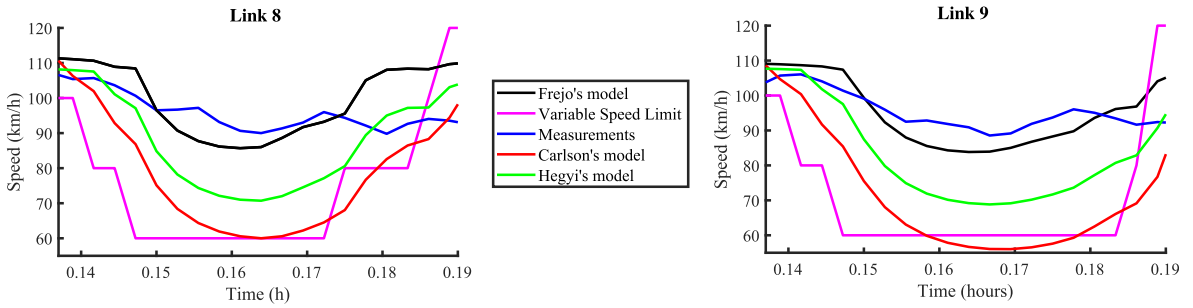


**Fig. 15.** Real and estimated speed for December 18 for Links 8 and 9: Measurements (blue), VSL (magenta), Carlson's model (red), Hegyi's model (green) and Frejo's model (black). (For interpretation of the references to colour in this figure legend, the reader is referred to the web version of this article.)

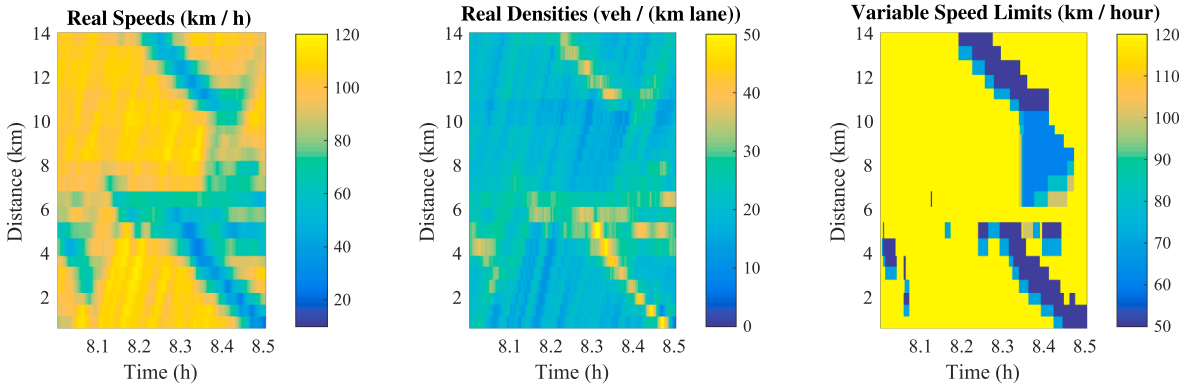


**Fig. 16.** Real speeds, densities, and VSLs for October 30.

one observed for low densities in order to match the estimation for higher densities (see Fig. 8). Since Frejo's model reduces the estimated speeds when densities are increased, it is able to set the right value of the compliance parameter $\alpha_i$ for low densities.

For the second plotted scenario, Fig. 16 shows an activation of the SPECIALIST algorithm for links with higher (but smaller than the critical) densities (between 10 and 30 veh/ km lane). These plots correspond to October 30 from 8:00 to 8:30 AM. In this case, the VSL-induced speeds (shown in Fig. 17) are lower than for the previous case (December 18) because the densities are closer to the critical one. As expected, it can be seen that the speeds predicted by Frejo's model are smaller than for December18 due to the exponential form of the VSL-induced FD (as explained in Section VII) and, therefore, the model is able to properly approach the real measurements. On the other hand, the predictions given by Hegyi's and Carlson's models are again less accurate because the compliance is not properly modeled.

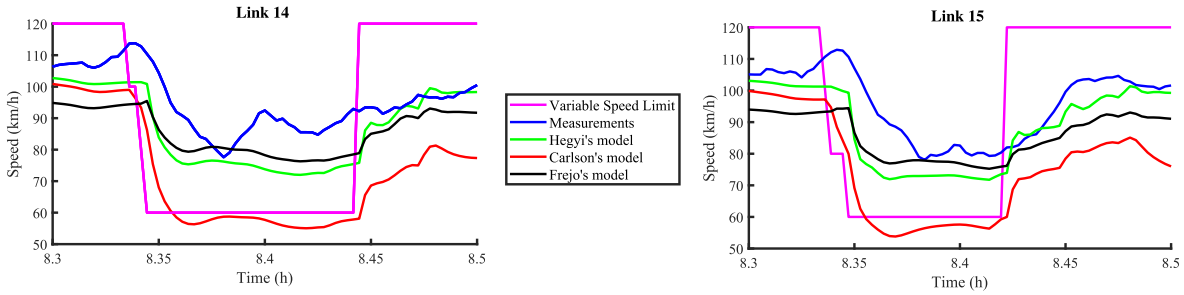


**Fig. 17.** Real and estimated speed for October 30 for Links 14 and 15: Measurements (blue), VSL (magenta), Carlson's model (red), Hegyi's model (green) and Frejo's model (black). (For interpretation of the references to colour in this figure legend, the reader is referred to the web version of this article.)

## 10. Conclusions

This paper has analyzed the effects of VSLs on freeway traffic flow based on the field data available from the A12 freeway in The Netherlands. In addition, we have proposed a new macroscopic model for VSLs (Frejo's model). The following conclusion have been drawn:

- As stated in previous references, the critical density of a link is increased if the corresponding VSL is decreased.
- For the studied scenario, the capacity of a link is reduced if the corresponding speed limit is decreased from 120 to 90 km/h (even though 90 km/h is above the critical speed).
- Carlson's and Frejo's model can be adapted in order to match any VSL-induced critical density and any VSL-induced capacity for each link. On the other hand, the lack of capability of Hegyi's model to be calibrated for different VSL-induced capacities and critical densities may be one of its main drawbacks.
- In order to properly model the VSL-induced free flow speed, a high value of $\alpha$ (compliance parameter) has to be used in some scenarios. Carlson's model considers than the VSL-induced free flow speed is equal to the actual VSL so this model is not able to properly model this kind of response with such a low compliance. However, if the VSLs are enforced, the corresponding compliance may be much higher and, therefore, Carlson's model would exhibit a more accurate prediction.
- When densities are increased, the VSL-induced speeds start to decrease substantially. Therefore, the use of an exponential equation for the FD increases the accuracy of the prediction and, therefore, triangular FDs (as used in Hegyi's model for the uncongested VSL-induced speed) entail a loss of prediction accuracy.
- For the scenario analyzed, the three models considered are able to properly estimate speeds with a great accuracy for both calibration and validation days.
- Better predictions (and so, lower mean speed errors) are obtained using Frejo's model (especially when VSLs are applied to uncongested links).

As in any other modeling problem, model choice will depend on the circumstances of each case. For example, if the VSLs are only going to be applied for very low densities in a freeway with full compliance, the three models are going to perform similarly. In this case, Hegyi's model would be the best choice (since it is the simplest of the three considered models). However, if the compliance is not high and the capacity is considerably reduced when VSLs are applied or if the desired speeds are considerably changing for different values of uncongested densities the use of Frejo's model is justified (especially from a control point of view).

## Acknowledgments

This research was supported by the European Union's Horizon 2020 research and innovation programme under the Marie Skłodowska-Curiegrant agreement No 702579 and by the European Research Council under the European Union's Seventh Framework Programme (FP/2007–2013) within the Project TRAMAN21 under Grant 321132. The authors are grateful to Andreas Hegyi and to the Dutch Ministry of Transport, Public Works, and Water Management - Rijkswaterstaat – Centre for Transport and Navigation for providing the traffic data.

## Appendix A. Supplementary material

Supplementary data associated with this article can be found, in the online version, at https://doi.org/10.1016/j.trc.2019.01.001.

## References

Camacho, E.F., Bordons, C., 2010. Model Predictive Control. Springer.
Carlson, R.C., Papamichail, I., Papageorgiou, M., Messmer, A., 2010. Optimal motorway traffic flow control involving variable speed limits and ramp metering.

Transport. Sci. 44 (2), 238–253.
Carlson, R.C., Papamichail, I., Papageorgiou, M., 2011. Local feedback-based mainstream traffic flow control on motorways using variable speed limits. IEEE Trans. Intell. Transp. Syst. 12 (4), 1261–1276.
Cremer, M., 1979. Der Verkehrsfluss aud Schnellstrassen. Springer-Verlag, Berlin.
Daganzo, C.F., 1994. The cell transmission model: a dynamic representation of highway traffic consistent with the hydrodynamic theory. Transport. Res. Part B: Methodol. 28 (4), 269–287.
Duret, A., Ahn, S., Buisson, C., 2012. Lane flow distribution on a three-lane freeway: general features and the effects of traffic controls. Transport. Res. Part C: Emerg. Technol. 24, 157–167.
Frejo, J.R.D., Camacho, E.F., 2012. Global versus local MPC algorithms in freeway traffic control with ramp metering and variable speed limits. IEEE Trans. Intell. Transp. Syst. 13 (4), 1556–1565.
Frejo, J.R.D., De Schutter, B., 2018. SPERT: A SPEed limit strategy for Recurrent Traffic jams. IEEE Trans. Intell. Transp. Syst. 1–12 Early Access.
Frejo, J.R.D., Núñez, A., De Schutter, B., Camacho, E.F., 2014. Hybrid model predictive control for freeway traffic using discrete speed limit signals. Transport. Res. Part C: Emerg. Technol. 46, 309–325.
Frejo, J.R.D., Papamichail, I., Papageorgiou, M., Camacho, E.F., 2016. Macroscopic modeling and control of reversible lanes on freeways. IEEE Trans. Intell. Transp. Syst. 17 (4), 948–959.
Frejo, J.R.D., Papamichail, I., Papageorgiou, M., De Schutter, B., 2018. A new macroscopic model for Variable Speed Limits. In: 15th IFAC Symposium on Control in Transportation Systems (CTS 2018), IFAC-PapersOnLine, vol. 51, no. 9, pp. 343–348.
Goldberg, D.E., 1989. Genetic Algorithms in Search, Optimization and Machine Learning. Addison-Wesley Longman Publishing Co.
Hegyi, A., Hoogendoorn, S.P., 2010. Dynamic speed limit control to resolve shock waves on freeways - Field test results of the SPECIALIST algorithm. In: 13th International IEEE Conference on Intelligent Transportation Systems, pp. 519–524.
Hegyi, A., De Schutter, B., Hellendoorn, H., 2004. Optimal coordination of variable speed limits to suppress shock waves. Transp. Res. Rec. 1852, 167–174.
Hegyi, A., De Schutter, B., Hellendoorn, H., 2005. Model predictive control for optimal coordination of ramp metering and variable speed limits. Transport. Res. Part C: Emerg. Technol. 13 (3), 185–209.
Hegyi, A., Hoogendoorn, S.P., Schreuder, M., Stoelhorst, H., Viti, F., 2008. SPECIALIST: a dynamic speed limit control algorithm based on shock wave theory. In: 11th International IEEE Conference on Intelligent Transportation Systems, pp. 827–832.
Heydecker, B.G., Addison, J.D., 2011. Analysis and modelling of traffic flow under variable speed limits. Transport. Res. Part C: Emerg. Technol. 19 (2), 206–217.
Knoop, V.L., Duret, A., Buisson, C., van Arem, B., 2010. Lane distribution of traffic near merging zones influence of variable speed limits. In: 13th International IEEE Conference on Intelligent Transportation Systems, pp. 485–490.
Lu, X., Shladover, S., 2014. Review of variable speed limits and advisories: theory, algorithms, and practice. Transport. Res. Rec.: J. Transport. Res. Board 2423, 15–23.
Nelder, J.A., Mead, R., 1965. A simplex method for function minimization. Comput. J. 7 (4), 308–313.
Papageorgiou, M., Hadj-Salem, H., Middelham, F., 1997. ALINEA local ramp metering: summary of field results. Transport. Res. Rec.: J. Transport. Res. Board 1603, 90–98.
Papageorgiou, M., Kosmatopoulos, E., Papamichail, I., 2008. Effects of variable speed limits on motorway traffic flow. Transport. Res. Rec.: J. Transport. Res. Board 2047, 37–48.
Papageorgiou, M., Papamichail, I., Messmer, A., Yibing, W., 2010. Traffic Simulation with METANET, Fundamentals of Traffic Simulation. Springer.
Papamichail, I., Kampitaki, K., Papageorgiou, M., Messmer, A., 2008. Integrated ramp metering and variable speed limit control of motorway traffic flow. In: 17th IFAC World Congress, vol. 41. pp. 14084–14089 2.
Robinson, M., 2000. Examples of variable speed limit applications. In: Speed Management, Workshop Notes, 79th Annual Meeting of Transportation Research Board.
Smulders, S., 1990. Control of freeway traffic flow by variable speed signs. Transport. Res. Part B: Methodol. 24 (2), 111–132.
Soriguera, F., Martínez, I., Sala, M., Menéndez, M., 2016. Effects of dynamic speed limits on a Dutch freeway. Transport. Res. Rec.: J. Transport. Res. Board 2560, 87–96.
Soriguera, F., Martínez, I., Sala, M., Menéndez, M., 2017. Effects of low speed limits on freeway traffic flow. Transport. Res. Part C: Emerg. Technol. 77, 257–274.
Spiliopoulou, A., Papamichail, I., Papageorgiou, M., Chrysoulakis, J., July 2014. CALISTO user's manual, Deliverable 4.1. Technical Report for the Project SMOOTH, ARCHIMEDES III, Athens.
Spiliopoulou, A., Papamichail, I., Papageorgiou, M., Tyrinopoulos, Y., Chrysoulakis, J., 2017. Macroscopic traffic flow model calibration using different optimization algorithms. Int. J. Oper. Res. 17, 146–164.
Sumner, R.L., Andrew, C.M., 1990. Variable Speed Limit System, Report FHWA-RD-89-001. FHWA, U.S. Department of Transportation.
van den Hoogen, E., Smulders, S., 1994. Control by variable speed signs: results of the Dutch experiment. In: Seventh International Conference on Road Traffic Monitoring and Control, pp. 145–149.
Wang, Y., Papageorgiou, M., Sarros, G., Knibbe, W.J., 2006. Real-time route guidance for large-scale express ring-roads. In: 9th International IEEE Intelligent Transportation Systems Conference, pp. 224–229.
Yuan, K., Knoop, V.L., Hoogendoorn, S.P., 2015. Capacity drop: relationship between speed in congestion and the queue discharge rate. Transport. Res. Rec.: J. Transport. Res. Board 2491, 72–80.
Zackor, H., 1972. Beurteilung verkehrsabhängiger Geschwindigkeitsbeschränkungen auf Autobahnen. Strassenbau Strassenverkehrstech 128, 1–61.
Zegeye, S.K., De Schutter, B., Hellendoorn, J., Breunesse, E.A., Hegyi, A., 2012. A predictive traffic controller for sustainable mobility using parameterized control policies. IEEE Trans. Intell. Transp. Syst. 13 (3), 1420–1429.